RSC Advances

ROYAL SOCIETY OF CHEMISTRY

www.rsc.org/advances

RSC Advances

RSCPublishing

PAPER

Highly Efficient Removal of ^{137}Cs in Seawater by Potassium Titanium Ferrocyanide Functionalized Magnetic Microspheres with Multilayer Core-shell Structure

Cite this: DOI: 10.1039/x0xx00000x

Rong Yi, Gang Ye,* Fengcheng Wu, Mingfen Wen, Xiaogui Feng, and Jing Chen*

Received 00th January 2014,
Accepted 00th January 2014

DOI: 10.1039/x0xx00000x

www.rsc.org/

In this study, a novel kind of core-shell structured magnetic microspheres functionalized with potassium titanium ferrocyanide (KTiFC) was developed for highly efficient removal of radioactive cesium from seawater. During the synthesis, a compact silica protective interlayer was deliberately constructed to stabilize the nano-sized magnetite cores, while preventing the erosion under harsh environmental conditions. Due to high ion exchange capacity of the KTiFC functional layer, the magnetic microspheres exhibited high removal efficiency (≥ 97.7%) of radiocesium from ^{137}Cs-spike solutions (3000-35000 Bq/L) and contaminated seawater. Batch experiments revealed that adsorption equilibrium was rapidly reached within 30 min and the maximum adsorption capacity was up to 43.09 mg/g. Kinetic models and Langmuir/Freundlich adsorption isotherm equations were used to fit the experiment data for describing the adsorption process. Owing to the favorable magnetic property, a facile separation and reclamation of the magnetic microspheres from aqueous solution was achieved under external magnetic field. Moreover, from a practical viewpoint, the magnetic microspheres were proved to have good re-dispersion property and long-term stability against strong HNO_3 solution (1.0 mol/L). These magnetic microspheres are believed to hold great promise for the clean-up of radiocesium contaminated water around nuclear facilities and/or in nuclear accidents.

Introduction

Substantial amounts of radioactive contaminations containing harmful fission products (FPs) are generated during the operation of nuclear facilities every year. Due to their long-term threat to the ecosystem and human health, the detection and separation of these hazards has been a world-wide concerned issue. Among the FPs, radiocesium is a major component widely present in radioactive liquid waste and has been involved in nuclear accidents in the past years[1]. After the Fukushima Daiichi nuclear disaster in 2011, excessive level of ^{137}Cs (half-life 30.2 years) was detected in the seawater along the coastline of Fukushima prefecture[2]. ^{137}Cs is a strong gamma emitter with high solubility, which enhances its migration through groundwater to the biosphere. Meanwhile, because of its chemical similarity to potassium, ^{137}Cs can be easily incorporated in terrestrial and aquatic organisms[3]. For these reasons, recently, numerous efforts have been made to seek out effective and eco-friendly methods for the removal of radiocesium from contaminated aqueous media[4-6].

Ion exchange[7] has been a well-established method to separate and recover cesium from waste solutions. As a good class of inorganic ion exchanger, transition metal ferrocyanides have shown excellent adsorption ability towards cesium because of their high affinity to Cs(I) in solutions[8,9]. However, inadequate strength and unsuitable mechanical properties are major disadvantages of these sorbent materials which rendered them unsuitable for the industrial applications[10,11]. For example, granular particles or slimes essential for liquid flow through columns are difficult to obtain by a simple precipitation reaction between soluble ferrocyanides and salts of divalent transition metals. To overcome these shortcomings, different types of support materials, such as polymers[12], biopolymers[13], colloid[11], anion exchanger resin[14], mineral oxide[15], porous silica gel particles[16], were employed for the binding/deposition of the ferrocyanides, which could then readily reduce the clogging effect and excessive pressure drop during the operation of fix-bed columns. However, the introduction of matrix materials inevitably sacrificed the operational simplicity and economic efficiency in column separation.

In recent years, magnetic nanoparticles (MNPs) have emerged as a fascinating functional material which combines the advantages of nanomaterials with the facility of magnetic separation. Due to the unique magnetic responsivity, low cytotoxicity, and chemically-modifiable surface property[17], MNPs possess great potential in bioseparation[18,19], environmental remediation[20], catalysis[21], enzyme immobilization[22,23], magnetic resonance imaging[24], etc. Lately, functionalization of the MNPs with transition metal ferrocyanides by

deposition or coating paves a way for the facile separation of cesium. Reports show that Prussian blue and potassium nickel (II) hexacyanoferrate (II) modified MNPs have been prepared with favorable magnetism and good adsorption ability, which allowed an effective remediation of Cs-contaminated environment[13,25-27]. Nevertheless, from a practical viewpoint, maintaining the stability of these magnetic composites is still quite challenging. Nano-sized particles tend to form agglomerates to minimize the surface energy[28]. Moreover, since the magnetic composites are mostly exposed to HNO_3-containing radioactive liquid waste for Cs adsorption, particle degradation and magnetic susceptibility reduction are unavoidable due to dissolution and leaching of the magnetite[29]. Fortunately, multilayer core-shell architecture, known as an appealing strategy for nanomaterials preparation, have offered substantial promise to solve this problem. Based upon this strategy, an impenetrable protective layer can be constructed in the magnetic composites, which will not only stabilize the nano-sized particles and prevent the damages from the external environment, but also provide many possibilities for further surface functionalization[30-33]. However, to our knowledge, the core-shell architecture strategy has never been employed for the synthesis of ferrocyanides modified MNPs.

In present study, we reported a novel kind of core-shell structured magnetic microsphere functionalized with potassium titanium ferrocyanide (KTiFC) for an effective decontamination of radiocesium. The magnetic composite exhibited high removal efficiency (≥ 97.7%) of radiocesium from ^{137}Cs-spike solutions (about 3000-35000 Bq/L) and contaminated seawater, and could be easily separated from aqueous solution under external magnetic field due to its favorable magnetic property. Moreover, owing to the introduction of a silica interlayer, the material was endowed with a good dispersion property and excellent stability against strong HNO_3 solution (1.0 mol/L). Structure, morphology, and magnetic properties were characterized by XRD, FT-IR, SEM and VSM. The adsorption behavior towards cesium including adsorption kinetics and adsorption isotherm was fully investigated.

Experimental section

Chemicals. Ferric chloride hexahydrate ($FeCl_3 \cdot 6H_2O$), anhydrous sodium acetate, Potassium ferrocyanide ($K_4Fe(CN)_6 \cdot 3H_2O$), ethylene glycol (EG), tetraethyl orthosilicate (TEOS), tetrabutyl orthotitanate (TBOT) and hydroxypropyl cellulose (HPC) were purchased from Sigma-Aldrich. Cocktail Ultima Gold AB (Perkin Elmer) and 20 mL polyethylene vials (Perkin Elmer) were employed for liquid scintillation counting (LSC) measurement. All other chemicals of analytical grade, including metal nitrates, nitric acid, ammonium hydroxide and other reagents, were commercially obtained and used without further purification. Deionized water was obtained from a Milli-Q water purification system. Cesium contaminated seawater was prepared by using the real seawater from both shallow and deep districts of Bohai Sea in China. Calculated amount of cesium was added to evaluate the adsorption ability of the materials.

Characterization. Morphology of the magnetic microspheres was investigated by using LEO 1530 scanning electron microscope (SEM) with an accelerating voltage of 20 kV, coupled with energy-dispersive X-ray spectroscopy (EDX) for determination of sample composition. Powder X-ray diffraction (XRD) patterns of the products were collected on a diffractometer with Cu K α radiation, with a scan step of 0.02° and a scan range between 10° and 80°. Fourier transform infrared (FT-IR) spectra were recorded on a Nicolet Nexus 470 spectrometer with KBr pellets in the range 4000-400 cm^{-1} at room temperature. Magnetic properties (M-H curve) were measured at 300 K by cycling the external field between -10 and 10 KOe using 730T Vibrating Sample Magnetometer (VSM). The concentration of the metal ions was determined by inductively coupled plasma mass spectrometry (ICP-MS). An ultra-low background liquid scintillation counting (Quantulus 1220) from Perkin Elmer was used for the measurements of radioactivity.

Synthesis of Fe_3O_4 magnetic core. The magnetic particles Fe_3O_4 were prepared through a solvothermal reaction[17]. Briefly, 2.70 g of $FeCl_3 \cdot 6H_2O$ and 7.2 g of sodium acetate were dissolved in 100 mL ethylene glyol under magnetic stirring. A homogeneous yellow solution was obtained and transferred into a Teflon-lined stainless-steel autoclave with capacity of 200 mL. The autoclave was sealed and heated at 200 °C for 8 h, followed by cooling to room temperature. The black magnetite particles were collected by magnet and washed several times with ethanol and deionized water. Finally, the product was dried in vacuum at 60 °C for 12 h.

Synthesis of Fe_3O_4@SiO_2 microspheres. Magnetite microspheres were coated with a thin silica layer through a sol-gel approach, forming Fe_3O_4@SiO_2 microspheres with core-shell structure. Typically, the magnetic Fe_3O_4 particles (0.5 g) were treated with 0.1 mol/L HCl aqueous solution by ultrasonication for 20 min. Then, the magnetite particles were washed with deionized water and dispersed in a mixture of absolute ethanol (200 mL), deionized water (50 mL) and concentrated ammonia aqueous solution (2.5 mL, 28 wt.%), followed by the injection of tetraethyl orthosilicate (TEOS, 0.5 mL). After stirring at room temperature for 6 h, the Fe_3O_4@SiO_2 microspheres were separated by use of a magnet, washed with ethanol and deionized water, and then dried in vacuum at 60 °C for 6 h.

Synthesis of Fe_3O_4@SiO_2@KTiFC. In a typical procedure, 0.5g Fe_3O_4@SiO_2 particles was mixed with deionized water (3 mL), HPC (1.25 g), and absolute ethanol (400 mL) under vigorous mechanical stirring. An ethanol solution (80 mL) of TBOT (5 mL) was added drop by drop followed by heating the solution at reflux at 85 °C for 150 min. The obtained product was separated with magnet, washed with ethanol several times and dried in vacuum at 60 °C for 6 h [21]. Then, the particles were soaked into 0.5 mol/L $K_4Fe(CN)_6$ containing 1.5 mol/L HCl. After mechanical stirred for 5h, the black particles were separated with the help of magnet and washed with deionized water until the washing liquor was colorless. Finally, the product Fe_3O_4@SiO_2@KTiFC was dried in vacuum at 60 °C for 10 h.

Adsorption kinetics. Adsorption kinetics were investigated by batch operation in 10 mL plastic tube immersed in 25 ºC constant temperature bath oscillator. The concentration of Cs(I) for kinetic study was 0.3 g/L. 10 mg of Fe_3O_4@SiO_2@KTiFC particles were adding into 4 mL of the above cesium-containing solution with HNO_3 concentration of 1.0 mol/L. The mixed liquor was shaken at about 180 rpm for different times (5-240 min). Then, the magnetic particles were separated by using an NdFeB magnet. The aqueous solution was filtered with syringe-type filters. The concentration of the residual cesium ions in the aqueous phase was measure by ICP-MS. Adsorption capacity q_t were used to evaluate the adsorption ability of the magnetic composite toward Cs (I). The q_t (mg/g) at time t was calculated by equation (1):

$$q_t = \frac{(C_0 - C_t) \times V}{M} \qquad (1)$$

where C_0 and C_t represent aqueous cesium concentration at the initial time and at the time t, respectively; V is the volume of solution, and M is the mass of adsorbent.

Adsorption isotherm. Adsorption isotherm was investigated based on batch experiments. The initial cesium concentration varied from 0.15-1.0 g/L. The Fe_3O_4@SiO_2@KTiFC particles were contacted with 4 mL of solution containing various concentration of cesium with shaking at swing bed for 2 h. After equilibrium, the

particles were separated, filtered and the residual cesium concentration were analyzed by ICP-MS.

Decontamination of radioactive ^{137}Cs solution. Solutions containing radioactive ^{137}Cs were prepared by diluting stock solution to the required concentrations. 20 mg of the Fe_3O_4@SiO_2@KTiFC particles was dispersed in 20 mL ^{137}Cs solution in a flask. After a gentle shaking of the flask for 90 min, solid-liquid separation was accomplished by a magnet. Aliquot of aqueous solution was filtered with syringe-type filter and added to a vial for the determination of activity by liquid scintillation counting (LSC). The measurement method has been elaborated in our previous publication[34]. Here, we briefly describe it as follows. 10 mL of Cocktail Ultima AB was added to a vial for background measurement in advance. Then, appropriate amount (*e.g.* 1 mL) of the ^{137}Cs solutions was added to the vial, followed by shaking to obtain a homogeneous mixture. The radioactivity of the ^{137}Cs solutions was measured and determined by deducting the background signal.

Remove rate R(%) and decontamination factor (DF) were used to assess the adsorption performance of Fe_3O_4@SiO_2@KTiFC particles towards ^{137}Cs, which were defined by following equations:

$$R = \frac{C_0 - C_e}{C_0} \times 100\% \qquad (2)$$

$$DF = \frac{A_0}{A_f} \qquad (3)$$

where A_0 and A_f were aqueous cesium radioactivity in initial solution and final solution after treatment with absorbent respectively.

Cesium removal from seawater. 5 mg of Fe_3O_4@SiO_2@KTiFC particles were allowed to contact with 4 mL of cesium contaminated seawater. After shaking for 2 h, the aqueous solution was removed and filtered with syringe-type filters. The initial and residual cesium concentration were analyzed by ICP-MS. Except for the remove rate R(%), distribution coefficient (K_d) was defined for evaluated the Cs removal ability of the particles from seawater:

$$K_d = \frac{C_0 - C_e}{C_e} \times \frac{V}{M} \qquad (4)$$

where C_e is the equilibrium concentration of Cs(I) in the seawater.

Results and discussions

Synthesis and Characterization of Fe_3O_4@SiO_2@KTiFC. Potassium titanium ferrocyanides (KTiFC) have been recognized as a favorite inorganic ion exchanger to be used for radiocesium clean-up. Here, by covalent deposition of KTiFC to the silica encapsulated magnetite particles, we combined the advantages of such ion exchanger with the convenience of magnetic separation, which resulted in a facile and efficient removal of cesium in contaminated solutions. The synthesis scheme of the Fe_3O_4@SiO_2@KTiFC core-shell structured microspheres is illustrated in Figure 1a. First, uniform magnetite microspheres with an average diameter of approximate 300 nm were obtained via a solvothermal synthesis. The micro-morphology of the product was examined by SEM as shown in Figure 1b. The well-formed magnetite core particles with good mechanical strength were then utilized for surface modification and/or functionalization. Through the typical Stöber method, a silica layer with the thickness about 20 nm was generated as a protective coating, which can be clearly observed in the TEM inset of Figure 1c.

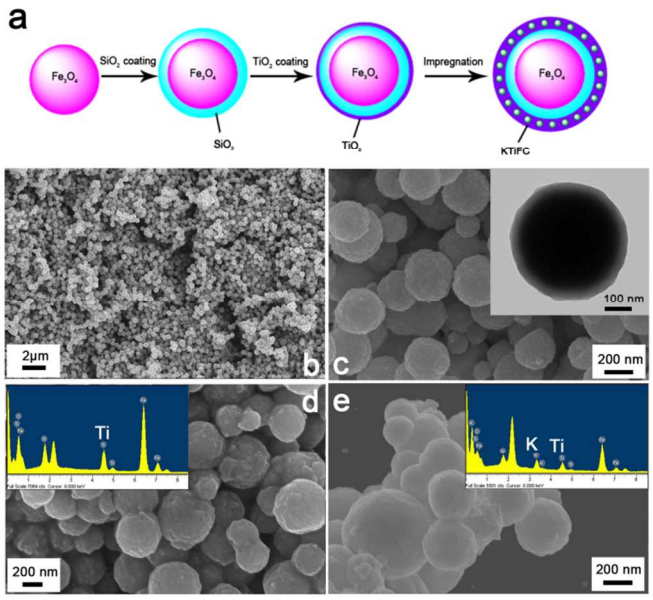

Figure 1. Schematic illustration of the fabrication procedure of Fe_3O_4@SiO_2@KTiFC (a), and SEM study of Fe_3O_4 (b), Fe_3O_4@SiO_2 microspheres (c), Fe_3O_4@SiO_2@TiO_2 microspheres (d) and Fe_3O_4@SiO_2@KTiFC (e). The insets show the TEM image (c) and EDS spectra (d & e) of the magnetic particles.

As mentioned above, a large amount of acid and salts co-exist in the cesium-containing radioactive liquid wastes. The introduction of silica protective layer is crucial to prevent the erosion of the magnetite cores. Meanwhile, the silica coating also provides a friendly surface for the subsequent deposition of KTiFC functional layer. To this end, a thin layer of amorphous TiO_2 was first deposited to the Fe_3O_4@SiO_2 microspheres by the hydrolysis of TBOT in the ethanol solution with the help of hydroxypropyl cellulose (HPC)[35]. The obtained Fe_3O_4@SiO_2@TiO_2 particles had a near-spherical appearance with a rough surface (Figure 1d).

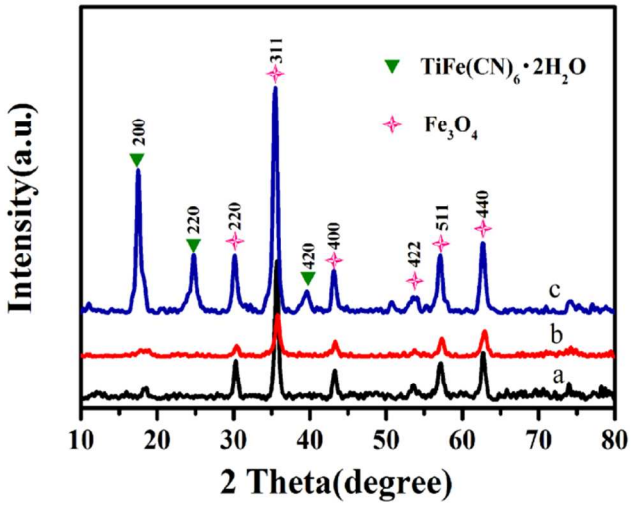

Figure 2. X-ray diffraction (XRD) patterns of Fe_3O_4@SiO_2 (a), Fe_3O_4@SiO_2@TiO_2 (b) and Fe_3O_4@SiO_2@KTiFC (c).

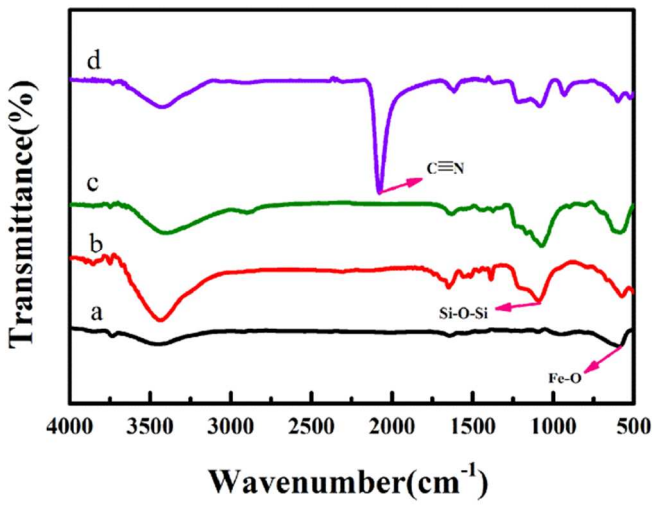

Figure 3. FT-IR spectra of Fe_3O_4 particles (a), Fe_3O_4@SiO_2 (b), Fe_3O_4@SiO_2@TiO_2 (c), and Fe_3O_4@SiO_2@KTiFC (d).

Evident Ti signal peak was observed in the EDS spectrum (Figure 1d, inset). Finally, the Fe_3O_4@SiO_2@TiO_2 particles were immersed into a mixed solution containing potassium ferrocyanide and hydrochloric acid. Under the precipitation reaction between TiO_2 and $Fe(CN)_6^{4-}$, potassium titanium ferrocyanides were formed on the surface of magnetic microspheres. Figure 1e shows the SEM image of the final Fe_3O_4@SiO_2@KTiFC particles. The presence of the Ti, K signal peaks in the EDS spectrum inset confirms the structure of the KTiFC functional layer.

The structure of Fe_3O_4@SiO_2@KTiFC particles were also verified by powder X-Ray diffraction (XRD) and Fourier transform infrared (FT-IR) spectra. Figure 2 shows the XRD patterns of Fe_3O_4@SiO_2 (a), Fe_3O_4 @SiO_2@TiO_2 (b) and Fe_3O_4@SiO_2@KTiFC (c). The diffraction peaks in curve (a) and (b) are in coincidence with a face center cubic Fe_3O_4 (JCPDS card 19-629). Obviously, after coating with the SiO_2 layer and TiO_2 layer, the diffraction patters of the obtained materials show no difference compared with pure magnetite, which indicates that both silica and titanium dioxide were in amorphous nature. The XRD patter of Fe_3O_4@SiO_2@KTiFC (curve c) reveals the superposition of diffractions of a magnetite phase and a $TiFe(CN)_6 \cdot 2H_2O$ phase. The (200) (220) and (420) reflections of $TiFe(CN)_6 \cdot 2H_2O$ phase are clearly observed, which matches well with previously study[36]. Meanwhile, an evident strong resonance at 2090 cm^{-1} is observed in the FT-IR spectrum of Fe_3O_4@SiO_2@KTiFC (Figure 3d) , which is the characteristic stretching vibration of cyanide groups, confirming the successful deposition of potassium titanium ferrocyanide on the surface of the Fe_3O_4@SiO_2 microspheres. Additionally, the typical adsorption bands at 582 cm^{-1} contributed by the stretching vibration of Fe-O band are found in all samples. Particles coated with a silica layer exhibit a strong Si-O-Si antisymmetric stretching vibration peak at 1089 cm^{-1} (Figure 3b-d). The signal of Si-O-Ti stretching vibration is around 950 cm^{-1}, which is partially overlapped by the broad Si-O peaks[21].

Magnetic properties. A vibrating magnetometer were be used to characterize the magnetic properties at 300 K. Figure 4A displays the magnetic hysteresis loops of Fe_3O_4 (a), Fe_3O_4@SiO_2 (b), Fe_3O_4@SiO_2@TiO_2 (c), Fe_3O_4@SiO_2@KTiFC (d). The saturation magnetization values of the magnetic composites are 80.4, 61.0, 44.1, 18.68 emu/g, respectively. The magnetite core and the silica encapsulated particles showed favorable magnetism, while the deposition of KTiFC resulted in a decrease of the saturation magnetization. Under the applied external magnetic field, the Fe_3O_4@SiO_2@KTiFC particles afford a sensitive response and can be quickly separated from the aqueous medium (Figure 4B). Moreover, negligible coercivity and remanence are observed from all of the hysteresis loops which confirmed the superparamagnetism of the magnetic particles. The superparamagnetic property will facilitate the stability and redispersion of the magnetic particles in solution, which is of great significance for practical magnetic separation applications.

Adsorption kinetic behavior. The effect of contact time on the adsorption capacity q_t of Fe_3O_4@SiO_2@KTiFC towards cesium was investigated in 1.0 mol/L HNO_3 solution containing 0.3 g/L of Cs(I). After different contact time intervals between 5 min and 4 h,

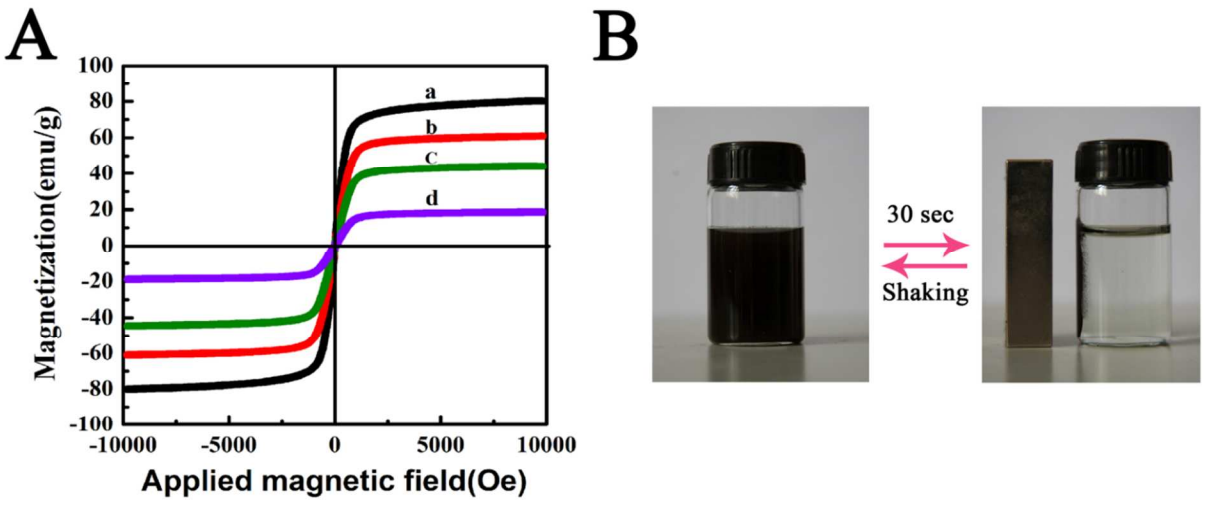

Figure 4. (A) Magnetic hysteresis loops of Fe_3O_4 particles (a), Fe_3O_4@SiO_2 (b), Fe_3O_4@SiO_2@TiO_2 (c), and Fe_3O_4@SiO_2@KTiFC (d); (B) magnetic separation-redispersion process of Fe_3O_4@SiO_2@KTiFC

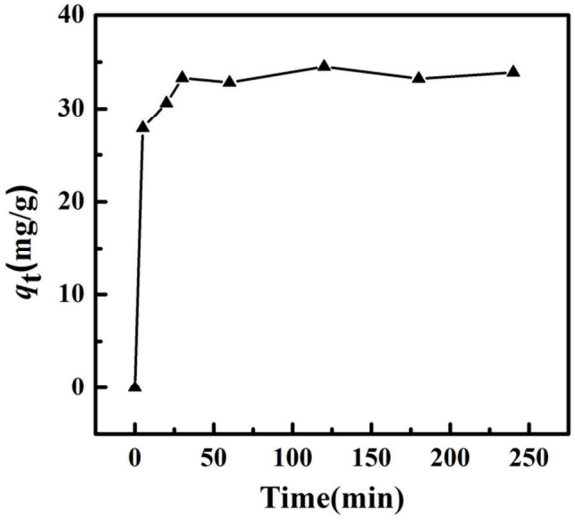

Figure 5. Influence of contact time on the adsorption capacity of cesium.

the mixture was separated and the aqueous cesium concentration was measured. The results are displayed in Figure 5. The curve reveals that cesium were adsorbed by KTiFC deposited magnetic materials fleetly and the equilibrium was established after 30 min with qt≈33.56 mg/g.

To better describe the adsorption of cesium by Fe_3O_4@SiO_2@KTiFC magnetic composite, two representative adsorption kinetic models including pseudo-first-order model[37] and pseudo-second-order model[38] were utilized to fit the experiment data. The related equation are given as Eq. (5-6):

$$\log(q_e - q_t) = \log(q_e) - \frac{k_1}{2.303}t \qquad (5)$$

$$\frac{t}{q_t} = \frac{1}{q_e}t + \frac{1}{k_2 q_e^2} \qquad (6)$$

where q_t and q_e are the adsorption capacity at equilibrium and at the time t (mg/g) , respectively. k_1 is the rate constant of pseudo-first-order model (1/min); k_2 is the rate constant of the pseudo-second-order model (g/μg min). Through fitting the experiment data by linear regression, the kinetic parameters k_1, k_2, q_e and the correlation coefficient R^2 were obtained and summarized in Table 1. Obviously, the results reveal that the Cs(I) adsorption process by Fe_3O_4@SiO_2@KTiFC magnetic composite was better described by a pseudo-second-order model. The fitted curve with R^2=0.999 is plotted in Figure 6. It can be inferred that the adsorption capacity is proportional to the number of active sites on the magnetic composite and the rate-limiting step may be chemical sorption or chemisorption

Table 1 Kinetic parameters fitted by pseudo-first-order model and pseudo-second-order model for cesium adsorption by Fe_3O_4@SiO_2@KTiFC magnetic composite.

Pseudo-first-order model			Pseudo-second-order model		
k_1 (min^{-1})	$q_{e,1}$ (mg/g)	R^2	k_2(g/mg min)	$q_{e,2}$ (mg/g)	R^2
0.368	33.08	0.989	0.024	33.98	0.999

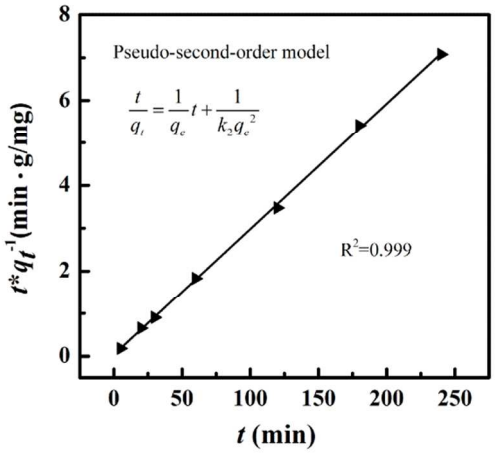

Figure 6. Pseudo-second-order model for adsorption of Cs(I) by Fe_3O_4@SiO_2@KTiFC.

involving valency forces through sharing or exchange of electrons between sorbent and sorbate[38-40].

Adsorption isotherm. The adsorption capacity of the Fe_3O_4@SiO_2@KTiFC magnetic microspheres as a function of cesium concentration was studied in batch experiments by altering the initial concentration from 0.15 to 1.0 g/L. Adsorption capacity q_e (mg/L) versus concentration of cesium after equilibrium C_e (g/L) was plotted in Figure 7. It is observed that adsorption capacity increased rapidly with the increase in Cs(I) ion concentration when the initial concentration of Cs(I) was less than 0.3 g/L, which may attributed to the fact that sufficient active sites were available[41]. While at the higher concentration, competition for available adsorption sites resulted in a gradual slowdown of increase in adsorption capacity.

The Langmuir and Freundlich adsorption isotherm models[42] were applied to fit the adsorption data at equilibrium. The Langmuir model is valid for single-layer adsorption with the hypothesis that all the binding sites are free. The nonlinear form of the equation is written as:

$$q_e = q_{\max}\frac{KC_e}{1+KC_e} \qquad (7)$$

where q_e and q_{max} are the equilibrium adsorption capacity and the monolayer maximum adsorption capacity (mg/g), respectively. K is a constant related to the affinity between the sorbent and sorbate.

In comparison, The Freundlich adsorption isotherm model is considered as empirical equation and used to describe multi-layer adsorption with several kinds of adsorption sites on the surface of sorbent. The model was in the following form:

$$q_e = K_F C_e^{1/n} \qquad (8)$$

where K_F and n are the Freundlich constants relative to the multilayer adsorption capacity and adsorption intensity, respectively. Figure 7 shows the experiments data and the curves fitted by The Langmuir and Freundlich models. It can be seen that the Langmuir model are more suitable for the description of the Cs(I) adsorption by Fe_3O_4@SiO_2@KTiFC. The fitted parameters and correlation coefficient for both models are listed in Table 2. The correlation

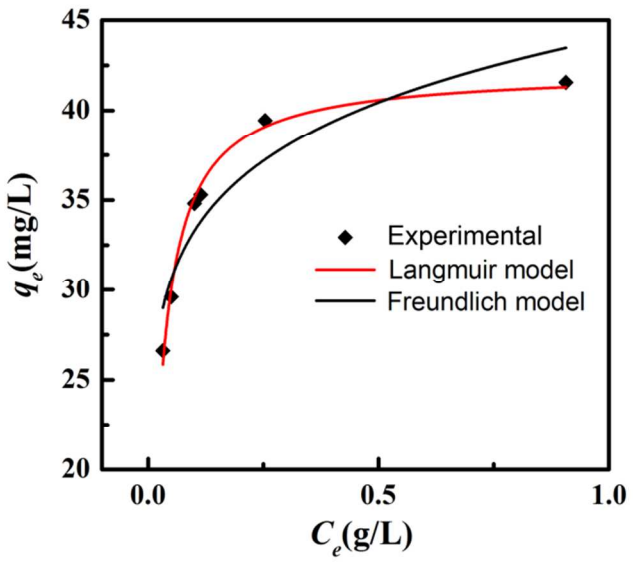

Figure 7. Experiment data and the fitted curves by Langmuir and Freundlich adsorption isotherm models.

coefficient R^2 for Langmuir model is up to 0.989. The maximum adsorption capacity of the Fe_3O_4@SiO_2@KTiFC magnetic microspheres towards Cs(I) is determined to 43.09 mg/g.

Table 2 Parameters of adsorption isotherms fitted by Langmuir and Freundlich models

Langmuir model			Freundlich model		
K_L (L/mg)	q_{max} (mg/g)	R^2	K_F	n	R^2
43.09	42.23	0.989	43.99	8.24	0.848

Selectivity. The selectivity of Fe_3O_4@SiO_2@KTiFC toward cesium was investigated in solution containing Cs(I) and other typical interference ions, such as Na(I), Ni(II), Fe(III), Sr(II), Mo(VI), Zr(IV), Ba(II), Nd(III). The solution was prepared to simulate a real acidic radioactive liquid waste with different initial concentrations for each ion[43]. The contact time was 2 h, and the phase ratio was 0.02 g/mL. After the adsorption, the residual metal ions in the solution were measured. The distribution coefficient (K_d) was calculated as summarized in Table 3. Obviously, the Fe_3O_4@SiO_2@KTiFC particles showed selective adsorption toward Cs(I) in the simulated radioactive liquid waste with the highest K_d (7849.8 mL/g). In comparison, the K_d values for all the interference ions were less than 10 mL/g. It is noteworthy that the concentration of K(I) showed a significant rise after the treatment with Fe_3O_4@SiO_2@KTiFC. This suggested that the ion exchange mechanism between K(I) and Cs(I) was responsible for the adsorption ability of the potassium titanium ferrocyanide[8]. The Cs(I) replaced the K(I) in the crystalline structures of cyanometallates, while the latter was released into the solution. Due to the size mismatch and charge unbalance, most of the interference ions could not be inserted into the crystalline structure[9].

Table 3 Selectivity of Fe_3O_4@SiO_2@KTiFC toward Cs(I)

Ions	Concentration (g/L)		K_d (mL/g)
	Initial	Treatment	
Cs^+	0.405	0.003	7849.8
Ni^{2+}	0.281	0.254	5.5
Fe^{3+}	0.240	0.239	0.1
Sr^{2+}	0.157	0.157	0.0
Mo^{6+}	1.805	1.717	2.6
Zr^{4+}	0.129	0.124	2.0
Ba^{2+}	0.405	0.379	3.4
Nd^{4+}	2.170	2.104	1.6
Na^+	1.138	1.112	2.5
K^+	0.002	**1.457**	/

Radioactive ^{137}Cs decontamination. The adsorption ability of the Fe_3O_4@SiO_2@KTiFC magnetic composite in radioactive ^{137}Cs-spiked solutions with different initial activity were examined. The performance parameters including decontamination factor (*DF*) and removal efficiency (*R*%) were obtained as summarized in Table 4. It can be seen that, the ^{137}Cs activity in the solutions shows a significant decrease after contact with the particles for 90 min. The removal efficiency, which exceeded 97% under all the experiment conditions, indicates the high adsorption competence of Fe_3O_4@SiO_2@KTiFC magnetic composite for ^{137}Cs decontamination. It is notable that the residual activity of ^{137}Cs solution after treatment with Fe_3O_4@SiO_2@KTiFC was 38 Bq/L at the initial concentration of 2993 Bq/L, which was a little bit higher than background activity. Besides, high *DF* (>40) further confirms the application potential of the Fe_3O_4@SiO_2@KTiFC magnetic composite for decontamination of ^{137}Cs-containing radioactive liquid wastes.

Table 4 Adsorption performance of Fe_3O_4@SiO_2@KTiFC in ^{137}Cs-spiked solutions

Activity of ^{137}Cs		Performance parameters	
A_0 (Bq/L)	A_f (Bq/L)	*DF* A_0/A_f	R (%)
2993	38	79	98.7
5347	48	112	99.1
16901	389	43	97.7
34244	437	78	98.7

A_0: Initial activity; A_f: final activity after treatment

Cesium removal from seawater. As mentioned above, radionuclide-contaminated seawater in Fukushima accident was a serious environmental concern. Due to the extremely low amount as well as the co-existence of a great number of competing metal ions, the removal of cesium in seawater remains a quite challenging task. In our study, real seawater from different districts of Bohai Sea in China was employed to prepare the cesium contaminated water for batch adsorption. The removal efficiency (*R*%) and distribution coefficient (K_d) were obtained in Table 5. For the shallow-ocean

seawaters with the addition of 15- or 150-fold cesium, the Fe_3O_4@SiO_2@KTiFC magnetic composite showed a removal efficiency higher than 98%, and the K_d was higher than 104 mL/g. After the treatment, cesium amount in the contaminated seawater was reduced lower than the background level. Similar results were obtained for the deep-ocean seawater, even though it had lower concentration of cesium.

Table 5 Adsorption performance of Fe_3O_4@SiO_2@KTiFC in cesium contaminated seawater

Solution	Cs(I) concentration (ppb)		R(%)	K_d(mL/g)
	Initial	Treatment		
shallow-ocean water	10.01	2.61	73.9	2100.2
shallow-ocean water + 0.15 ppm Cs(I)	161.35	2.52	98.4	48580.8
shallow-ocean water + 1.5 ppm Cs(I)	1603.5	8.28	99.5	151197.2
Deep-ocean water	2.58	1.23	52.5	834.8
Deep-ocean water +0.15 ppm Cs(I)	162	5.46	96.6	22507.9
Deep-ocean water +1.5 ppm Cs(I)	1660.5	11.25	99.3	112769.2

Stability evaluation in HNO_3 medium. As is known to us, a large amount of acid co-exists with radiocesium in radioactive liquid wastes. From the point of practical use, it is essential to evaluate the acid-resistance performance of Fe_3O_4@SiO_2@KTiFC magnetic composite in harsh acidic condition. For this purpose, 30 mg of the magnetic composite was soaked into 20 mL of 1.0 mol/L nitric acid solution. After shaking for different interval time, aliquots of liquid solution were removed for the determination of Fe^{3+} concentration in aqueous phase through spectrophotometry. Figure 8 gives the variation of the leached Fe^{3+} in the solution during 168 hours treatment. It can be seen that the naked Fe_3O_4 particles without a silica protective layer showed a fast degradation under the experimental condition. On the contrary, the Fe_3O_4@SiO_2@KTiFC magnetic composite with a silica protective layer was stable enough in strong acid condition. No detectable Fe^{3+} ions were found in the leaching solution. Therefore, it is believed that the Fe_3O_4@SiO_2@KTiFC magnetic microspheres should be stable enough for practical applications.

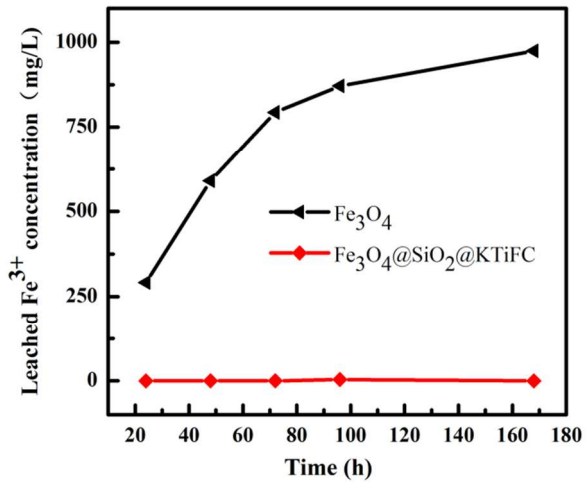

Figure 8. Acid-resistance test of the magnetite microspheres and Fe_3O_4@SiO_2@KTiFC particles.

Conclusions

A novel kind of potassium titanium ferrocyanide (KTiFC) functionalized magnetic microspheres was synthesized through a core-shell architecture strategy for the removal of radiocesium. The structure, morphology, and adsorption behavior of the Fe_3O_4@SiO_2@KTiFC magnetic composite were comprehensively studied. The high ion exchange efficiency of KTiFC in combination of the ease of the magnetic separation provided a facile way for the cesium decontamination. The magnetic composite showed high removal efficiency even in seawater containing extremely low concentration of cesium. Moreover, from a practical angle, the material has been proved to have excellent stability in strong HNO_3 solution due to the existence of silica coating as protection layer. It is optimistic that the magnetic composite is promising to be applied for the cleanup of radioactive cesium in contaminated environment.

Acknowledgements

The study was supported by Program for Changjiang Scholars and Innovative Research Team in University (IRT13026), and National Natural Science Foundation of China under Project 51103079 and 9122611.

Notes and references

Institute of Nuclear and New energy Technology, Tsinghua University, Beijing, P.R. China. Email: yegang@tsinghua.edu.cn; jingxia@tsinghua.edu.cn.

1 C. Liu, Y. Huang, N. Naismith, J. Economy and J. Talbott, *Environ. Sci. Technol*, 2003, **37**, 4261.
2 H. Kawamura, T. Kobayashi, A. Furuno, T. In, Y. Ishikawa, T. Nakayama, S. Shima and T. Awaji, *J. Nucl. Sci. Technol*, 2011, **48**, 1349.
3 R. R. Sheha, *J. Colloid. Interf. Sci*, 2012, **388**, 21.
4 P. K. Mohapatra, D. S. Lakshmi, A. Bhattacharyya and V. K. Manchanda, *J. Hazard. Mater*, 2009, **169**, 472.
5 A. Y. Zhang and Z. F. Chai, *Ind. Eng. Chem. Res*, 2012, **51**, 6196.
6 Y. X. Leng, G. Ye, J. Xu, J. Wei, J. C. Wang and J. Chen, *J. Sol-Gel Sci. Techn*, 2013, **66**, 413.
7 T. Sangvanich, V. Sukwarotwat, R. J. Wiacek, R. M. Grudzien, G. E. Fryxell, R. S. Addleman, C. Timchalk and W. Yantasee, *J. Hazard. Mater*, 2010, **182**, 225.
8 P. A. Haas, *Sep. Sci. Technol*, 1993, **28**, 2479.
9 C. Delchet, A. Tokarev, X. Dumail, G. Toquer, Y. Barre, Y. Guari, C. Guerin, J. Larionova and A. Grandjean, *RSC Adv*, 2012, **2**, 5707.
10 A. Nilchi, A. Khanchi, H. Atashi, A. Bagheri and L. Nematollahi, *J. Hazard. Mater*, 2006, **137**, 1271.
11 V. Avramenko, S. Bratskaya, V. Zheleznov, I. Sheveleva, O. Voitenko and V. Sergienko, *J. Hazard. Mater*, 2011, **186**, 1343.
12 H. H. Someda, A. A. ElZahhar, M. K. Shehata and H. A. El-Naggar, *Sep. Purif. Technol*, 2002, **29**, 53.

13 C. Dwivedi, S. K. Pathak, M. Kumar, S. C. Tripathi and P. N. Bajaj, *RSC Adv*, 2013, **3**, 22102.
14 T. P. Valsala, S. C. Roy, G. S. J., J. Gabriel, K. Raj and V. Venugopal, *J. Hazard. Mater*, 2009, **166**, 1148.
15 A. V. Voronina, V. S. Semenishchev, E. V. Nogovitsyna and N. D. Betenekov, *J. Radioanal. Nucl. Chem*, 2013, **298**, 67.
16 T. Sangvanich, V. Sukwarotwat, R. J. Wiacek, R. M. Grudzien, G. E. Fryxell, R. S. Addleman, C. Timchalk and W. Yantasee, *J. Hazard. Mater*, 2010, **182**, 225.
17 A. Lu, E. L. Salabas, F. Schüth, *Angew. Chem. Int. Ed*, 2007, **46**, 1222.
18 H. Chen, C. Deng and X. Zhang, *Angew. Chem. Int. Ed*, 2010, **49**, 607.
19 S. Wu, N. Duan, X. Ma, Y. Xia, Y. Yu, Z. Wang, H, *Chem. Commun,* 2012*, **48**,* 4866.
20 Y. Zhao, J. Li, S. Zhang, H. Chen and D. Shao, *RSC Adv*, 2013, **3**, 18952.
21 M. Ye, Q. Zhang, Y. Hu, J. Ge, Z. Lu, L. He, Z. Chen and Y. Yin, *Chem. Eur. J*, 2010, **16**, 6243.
22 J. Huang, R. Zhao, H. Wang, W. Zhao and L. Ding, *Biotechnol Lett*, 2010, **32**, 817.
23 S. Xuan, F. Wang, X. Gong, S. Kong, J. C. Yu and K. C. Leung, *Chem. Commun*, 2011, **47**, 2514.
24 H. Tan, J. M. Xue, B. Shuter, X. Li and J. Wang, *Adv. Funct. Mater*, 2010, **20**, 722.
25 R. D. Ambashta, P. K. Wattal, S. Singh and D. Bahadur, *J. Magn. Magn. Mater*, 2003, **267**, 335.
26 C. Thammawong, P. Opaprakasit, P. Tangboriboonrat and P. Sreearunothai, *J. Nanopart. Res*, 2013, **15**,
27 H. Yang, L. Sun, J. Zhai, H. Li, Y. Zhao and H. Yu, *J. Mater. Chem. A*, 2014, **2**, 326.
28 S. Laurent, D. Forge, M. Port, A. Roch, C. Robic, L. V. Elst and R. N. Muller, *Chem. Rev*, 2008, **108**, 2064.
29 M. D. Kaminski and L. Nuñez, *Sep. Sci. Technol*, 2002, **37**, 3703.
30 M. F. Shao, F. Y. Ning, J. W. Zhao, M. Wei, D. G. Evans and X. Duan, *J. Am. Chem. Soc*, 2012, **134**, 1071.
31 Y. Deng, D. Qi, C. Deng, X. Zhang and D. Zhao, *J. Am. Chem. Soc*, 2007, **130**, 28.
32 R. Yi, G. Ye, D. Pan, F. Wu, M. Wen and J. Chen, *J. Mater. Chem. A*, 2014, **2**,6840
33 M. Kaur, A. Johnson, G. X. Tian, W. L. Jiang, L. F. Rao, A. Paszczynski and Y. Qiang, *Nano Energy*, 2013, **2**, 124.
34 X. Feng, Q. He, Z. Chen, X. Han and J. Guo, *Radiat Meas*, 2011, **46**, 533.
35 D. Q. L. I. Qiao Zhang and Y. Yin, *Angew. Chem. Int. Edit*, 2011, **123**, 7226.
36 X. Feng, S. Jing, Q. Wu, J. Chen and C. Song, *Chinese J Chem Eng*, 2007, **15**, 184.
37 Y. S. Ho and G. McKay, *Process Saf. Environ*, 1998, **76**, 332.
38 Y. S. Ho and G. McKay, *Process Biochem*, 1999, **34**, 451.
39 Y. S. Ho, *J. Hazard. Mater*, 2006, **136**, 681.
40 Y. S. Ho, *Water Res*, 2006, **40**, 119.
41 C. Dwivedi, A. Kumar, K. K. Singh, A. K. Juby, M. Kumar, P. K. Wattal and P. N. Bajaj, *J. Appl. Polym. Sci*, 2013, **129**, 152.
42 E. Njikam and S. Schiewer, *J. Hazard. Mater*, 2012, **213 − 214**, 242.
43 F. F. Bai, G. Ye, G. J. Chen, J. C. Wei, J. C. Wang and J. Chen, *React. Func. Polym*, 2013, **73**, 228.

RSC Advances

RSCPublishing

PAPER

Table of contents entry

Highly Efficient Removal of ^{137}Cs in Seawater by Potassium Titanium Ferrocyanide Functionalized Magnetic Microspheres with Multilayer Core-shell Structure

Rong Yi, Gang Ye, Fengcheng Wu, Mingfen Wen, Xiaogui Feng, Jing Chen**

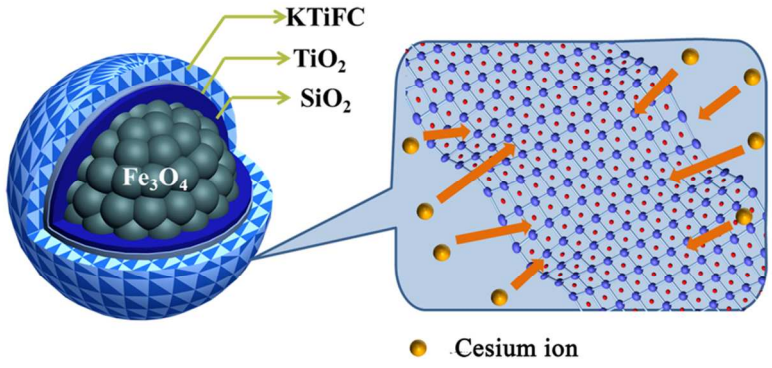

Transition metal ferrocyanides were deposited to the silica encapsulated magnetite particles for an effective decontamination of radiocesium.